Geochemistry, Geophysics, Geosystems

RESEARCH ARTICLE
10.1029/2020GC009254

Key Points:

- We compare laser ablation and solution-based ICP-MS Mg/Ca and Sr/Ca data generated on the same foraminifera shells
- Results show that both techniques yield comparable results, but depend on shell morphology and (for the laser analyses) the number of chambers analyzed
- We highlight potential issues in interpreting and comparing studies that use different analytical techniques

Correspondence to:
J. Fehrenbacher,
jennifer.fehrenbacher@oregonstate.edu

Citation:
Fehrenbacher, J., Marchitto, T., & Spero, H. J. (2020). Comparison of laser ablation and solution-based ICP-MS results for individual foraminifer Mg/Ca and Sr/Ca analyses. *Geochemistry, Geophysics, Geosystems*, *21*, e2020GC009254. https://doi.org/10.1029/2020GC009254

Received 22 JUN 2020
Accepted 20 OCT 2020

Comparison of Laser Ablation and Solution-Based ICP-MS Results for Individual Foraminifer Mg/Ca and Sr/Ca Analyses

Jennifer Fehrenbacher[1,2], Thomas Marchitto[3], and Howard J. Spero[2]

[1]College of Earth, Ocean, and Atmospheric Sciences, Oregon State University, Corvallis, OR, USA, [2]Department of Earth and Planetary Sciences, University of California Davis, Davis, CA, USA, [3]Department of Geological Sciences and Institute of Arctic and Alpine Research, University of Colorado Boulder, Boulder, CO, USA

Abstract The trace element and isotopic composition of foraminifera shells are widely used in paleoceanography to reconstruct past ocean conditions. Individual foraminifer analysis (IFA) is a rapidly expanding technique for obtaining trace element and/or isotope data from individual foraminifer specimens. IFA permits an assessment of population variability, which can be linked to environmental conditions at the time of calcification or can be used to assess postdepositional diagenesis. Uniform interpretation of IFA depends on the assumption that the data are not impacted by analytical technique. Here, we compare paired trace element (Mg/Ca and Sr/Ca) data for the same specimens analyzed first using laser ablation inductively coupled plasma-mass spectrometry (ICP-MS), followed by solution ICP-MS. Foraminiferal trace element (TE) to calcium ratios compare well between the two methods for foraminifera of simple morphology (*Orbulina universa*), heavily calcified specimens with TE-homogeneous outer calcite (*Pulleniatina obliquiloculata*), or when all chambers in multichambered species are analyzed by the laser and averaged together (*Trilobatus sacculifer* and *Neogloboquadrina dutertrei*). We highlight potential issues in interpreting and comparing studies that use different analytical techniques and recommend that the paleoceanographic community establish accepted protocols for generating IFA that would maximize our ability to cross-compare paleoceanographic data and reconstructions when different analytical techniques are used.

Plain Language Summary Foraminifera are sand-grained sized marine protists that form a calcite shell. They are ubiquitous in the ocean, their shells are commonly found in ocean sediments, and they are widely used to reconstruct past ocean conditions. Advancements in analytical capabilities over the past 2 decades now allow researchers to conduct geochemical analyses on individual foraminifer shells, often referred to as individual foraminifer analysis or IFA. IFA differs from past techniques because it sheds light on seasonal and depth-specific ocean conditions experienced by a population of individuals rather than average conditions when many shells are analyzed together. Here, we present data from two of the most commonly used procedures, laser ablation and solution analysis, to generate trace element data from the same individual shells in four foraminifera species and compare the results. We find that data from the two techniques compare well, but depend on shell morphology. For shells of simple morphology or those with heavily calcified outer calcite layers, either technique can be used and results can be readily cross compared. For foraminifera that have more complex morphologies, we suggest carefully designed sampling to ensure valid cross-comparison between studies that use one or the other technique.

1. Introduction

Trace element to calcium ratios (TE/Ca) measured in the calcite shells of planktic foraminifera are widely used to reconstruct past upper ocean conditions such as temperature (Barker et al., 2003; Cleroux et al., 2013; Sadekov et al., 2009) and seawater carbon chemistry (Babila et al., 2018; Henehan et al., 2013; Sosdian et al., 2018). Their utility in paleoceanographic research is made possible by the fact that the TE composition of foraminifera shells is modulated by environmental conditions at the time of calcification (e.g., Allen et al., 2016; Lea et al., 2000; Russell et al., 2004). Paleoceanographic studies typically combine large numbers of microfossils (up to 100) from each sediment core interval, sediment trap sample, or plankton tow to generate a single TE/Ca measurement (e.g., Dekens et al., 2002; Hollstein et al., 2017; Krupinski

et al., 2017). Such "bulk" solution TE analyses yield average population geochemistry for the material analyzed. However, there is a rich record of seasonal, interannual, and depth habitat information contained within populations that can only be explored with individual foraminifer analyses.

Advancements in analytical capabilities over the past 2 decades now allow researchers to conduct geochemical analyses on individual foraminifer specimens, often referred to as individual foraminifer analysis or IFA. IFA permits an assessment of population variability, which can be linked to environmental conditions at the time of calcification or to postdepositional diagenesis, with the acknowledgment that shell chemistry can vary even among individuals grown in identical laboratory conditions (de Nooijer et al., 2014; Spero et al., 2015). This approach was pioneered by Schiffelbein and Hills (1984) and used in early paleoceanographic applications with stable isotopes (Billups & Spero, 1996; Oba, 1990; Spero & Williams, 1990; Stott, 1992). More recent efforts have examined the effects of shell dissolution on TE/Ca ratios (Rongstad et al., 2017) and have explored the use of oxygen isotope and/or TE/Ca ratios from individual foraminifera in different populations to reconstruct ice sheet meltwater geochemistry (Vetter et al., 2017) or ENSO dynamics (Ford et al., 2015; Koutavas & Joanides, 2012; Rongstad et al., 2020; Rustic et al., 2015; Schmitt et al., 2019; Thirumalai et al., 2013; White et al., 2018).

Trace element IFA can be achieved through solution-based inductively coupled plasma-mass spectrometry (ICP-MS), laser ablation ICP-MS, or via thin section sampling techniques such as NanoSIMS and electron microprobe analysis (EMPA). Solution and LA-based ICP-MS analyses are commonly applied in paleoceanographic reconstructions whereas NanoSIMS and EMPA are typically used to explore mechanisms responsible for intrashell trace element variability (Eggins et al., 2004; J. Fehrenbacher and Martin, 2014; Jonkers et al., 2016; Kunioka et al., 2006; Sadekov et al., 2005). With solution-based IFA, specimens are analyzed whole, thereby averaging all chambers formed during ontogeny (e.g., Groeneveld et al., 2019; Rongstad et al., 2017). In contrast, LA-ICP-MS IFA utilizes laser spot analyses of either specific chambers or analyses of many chambers which are then combined to calculate an average TE/Ca value for a single specimen (Evans et al., 2016; Jonkers et al., 2012; Marr et al., 2013; Wit et al., 2010).

With the expanding use of different techniques for TE analyses on individual foraminifera shells, there is a clear need to cross calibrate data collected by LA-ICP-MS and solution-based techniques as no matrix-matched standards are currently available for this purpose. Here, we compare the Mg/Ca and Sr/Ca ratios of individual foraminifer specimens that were first analyzed by LA-ICP-MS and then subsequently analyzed using solution-based ICP-MS. Mg/Ca is a valuable paleotemperature proxy and the TE most widely measured in foraminiferal calcite. While foraminiferal Sr/Ca is not as widely interpreted in paleoceanographic research, it is very routinely measured along with Mg/Ca, thus the comparison is of interest. We explore differences in average TE/Ca ratios and population geochemistry obtained using both methods. We discuss the implications of interpreting data derived from IFA and assumptions that must be considered if only a single individual chamber or a subset of chambers are analyzed using laser ablation IFA.

2. Methods

2.1. Species and Sampling Strategy

We chose species for analysis with a range of morphologies, trace element variability, and ecological habitats that include *Orbulina universa*, *Pulleniatina obliquiloculata*, *Trilobatus sacculifer* (without the final sac-like chamber), and *Neogloboquadrina dutertrei*. *O. universa* and *T. sacculifer* are mixed-layer spinose species that possess dinoflagellate symbionts (Be et al., 1977; Gastrich, 1987). The final-stage morphology of *O. universa* is a single large spherical chamber that comprises 90% of the shell mass (Spero, 1988) and contains similar trace element heterogeneity around the entire shell (Bonnin et al., 2019). *T. sacculifer* is multichambered and has three chambers in the final whorl. *P. obliquiloculata* and *N. dutertrei* are multichambered thermocline dwelling nonspinose species that contain intracellular algal symbionts (Bird et al., 2018; Gastrich, 1987). *P. obliquiloculata* forms a thick cortex at the end of its ontogeny. The cortex has similar thickness in successive chambers and can represent an average of 32% of the shell wall thickness (Steinhardt et al., 2015). *N. dutertrei* typically form a crust that varies in thickness between chambers, where older chambers are thickest and progressively thin toward the final chamber (Jonkers et al., 2012; Steinhardt et al., 2015).

Foraminifera were picked from the 350–450 μm size fraction of the 18–20 cm interval (early Holocene) in core MW91-9 6GGC (2°12.54′S 156°57.9′E; 1.6 km depth). The core is located on the Ontong Java Plateau and is well above the regional lysocline (Hales, 2003; McCorkle et al., 1995), which largely eliminates changes in TE/Ca ratios due to dissolution on the seafloor (Dekens et al., 2002; Regenberg et al., 2014). The sedimentation rate in this location is 1–2 cm/1,000 years, thus the 2 cm interval sample represents a minimum of 500–1,000 years of sedimentation, likely longer due to the effects of bioturbation.

2.2. LA-ICP-MS Analysis

2.2.1. Sample Preparation for LA-ICP-MS

Specimens were rinsed (2x in ultrapure water, then 3x methanol, followed by 2x in ultrapure water) to remove finely adhering clays. Specimens were gently sonicated for 10 s during each rinse step. Rinses were followed by an oxidative cleaning step to remove any remnant organic matter from the outer whorl. This involved submersing the shells in a hot (65°C) mixture of 30% H_2O_2 buffered with 0.1 N NaOH for 10 min, during which samples were sonicated briefly for 10 s. The oxidative solution was then aspirated and the shells were rinsed 3x in ultrapure water. Specimens were dried in a fume hood and then transferred onto a slide prepared with double-sided carbon tape. *O. universa* shells were first cracked open under a microscope using a surgical scalpel (Shuxi & Shackleton, 1990) and a small fragment was transferred to the double-sided tape with the inner surface facing up. *T. sacculifer* shells were placed on the carbon tape with the aperture side up. *N. dutertrei* were placed on the carbon tape with the aperture side down. *P. obliquiloculata* were oriented randomly on the carbon tape.

2.2.2. Laser Ablation Protocol

Specimens were analyzed by LA-ICP-MS depth profiling (spot analysis) at the UC Davis Department of Earth and Planetary Sciences Stable Isotope Laboratory. Acquisitions were performed from the outer to inner surfaces on all species except *O. universa*, which were analyzed from the inside-to-outside. *O. universa* fragments were analyzed 2–3x. The final three chambers of *T. sacculifer* were analyzed 1–3x each. For *N. dutertrei*, depending on the orientation of the shell, 4–6 chambers were analyzed. Repeat analyses were obtained on chambers of *N. dutertrei* and *T. sacculifer* that were large enough to permit multiple laser spots. The *P. obliquiloculata* specimens had a moderately thick cortex which made the identification of individual chambers difficult during LA analysis, therefore 2–3 spots were analyzed in random locations on the shell. After LA analysis was complete, specimens were removed from the tape using methanol. Specimens were subsequently analyzed using solution-based ICP-MS analysis (see Section 2.3).

LA-ICP-MS analytical settings are summarized in Table 1. Eleven isotopes were measured using a rapid peak hopping procedure. Here we report only the Mg/Ca and Sr/Ca ratios. NIST SRM glass standards (610, 612, and 614) were analyzed periodically during the data collection period. Following our laboratory protocols, we analyzed a fossil *O. universa* to assess Mg/Ca and Sr/Ca reproducibility within and between analytical sessions (Fehrenbacher et al., 2015). A total of 22 replicate analyses were obtained from the same fossil *O. universa* between October 2013 and June 2015. The mean Mg/Ca ratio from these repeat measurements is 7.12 ± 0.4 mmol/mol (1σ). The mean Sr/Ca ratio from these repeat measurements is 1.34 ± 0.06 mmol/mol (1σ).

2.2.3. Laser Data Processing

TE/Ca were calculated offline in LA-Tools (Branson et al., 2019), a Python-based laser data reduction program. LA-Tools follows established data reduction protocols (Longerich et al., 1996) including screening for outliers (using an exponential decay despiking protocol and signal smoothing), drift correction by bracketing samples with NIST SRM analyses (610, 612, and 614), and subtracting average background counts from each data point. We used Al/Ca to screen for clay contamination and excluded data with Al/Ca ratios that exceed 0.4 nmol/mol. The mean TE/Ca for each profile is calculated by normalization to the known trace element concentrations in the drift-corrected NIST SRM standards (Jochum et al., 2011). ^{43}Ca was used as an internal standard. Individual chamber TE/Ca averages were obtained by integrating TE/Ca ratios throughout the depth profile, after excluding high TE/Ca ratios often encountered at the beginning of the ablation (e.g., Figure S1A in Fehrenbacher et al., 2018).

Table 1
Summary of Operating Conditions for the Laser Analyses

Agilent 7700x ICP-MS operating conditions	
RF Power	1500W
Argon (carrier) gas	1.05 lpm
Ar coolant gas flow	15 lpm
Ar auxiliary gas flow	1 lpm
Isotopes	^{11}B, ^{24}Mg, ^{25}Mg, ^{27}Al, ^{43}Ca, ^{44}Ca, ^{55}Mn, ^{66}Zn, ^{88}Sr, ^{138}Ba, ^{238}U
Dwell time per mass	Variable: 10 ms–50 ms
Total sweep time	424 ms
Photon Machines Analyte G2 UV Excimer operating conditions	
He gas flow	1.05 lpm
ThO^+/Th^+	<0.4%
Laser pulse rate	5 Hz
Energy	1.24 J/cm; 1.67 J/cm (*P. obliquiloculata* only)
Spot size	50–65 μm

2.2.4. Calculating Average Shell TE/Ca Ratios

Whole shell averages for *O. universa* and *P. obliquiloculata* were calculated by averaging the TE/Ca of the repeat analyses on each shell. For the multichambered species *T. sacculifer* and *N. dutertrei*, nonweighted and weighted whole shell averages were calculated. The nonweighted average was calculated by taking the chamber averages (i.e., the average TE/Ca of all repeat analyses on the same chamber) and giving them equal weight. For example, if a *T. sacculifer* specimen was analyzed 2x each on the F and F-1 chambers and 1x on the F-2 chamber. The whole shell average would be calculated as follows $((F_{TE/Ca\text{-}ratio} + F_{TE/Ca\text{-}ratio})/2 + (F\text{-}1_{TE/Ca\text{-}ratio} + F\text{-}1_{TE/Ca\text{-}ratio})/2 + F\text{-}2_{TE/Ca\text{-}ratio})/3$. The nonweighted average assumes that each chamber contributes the same amount of calcite to the shell average. In most multichambered species, chambers vary in size and thickness, therefore each chamber likely does not contribute the same amount of calcite to the shell average. We attempt to take this into account by calculating a weighted average based upon ablation time, which varies as a function of chamber thickness as long as the energy and repetition rate are consistent from spot to spot. We first calculate the TE/Ca ratio of each chamber, then sum the total amount of time each shell took to ablate, and weight the chambers based upon the ablation time. For example, the F, F-1, and F-2 chambers of sample S1 took an average of 37, 57, and 75 s to ablate, respectively, for a total of 168 s. The weighted whole shell average is then: $F_{TE/Ca\text{-}ratio} \times (37/168) + F\text{-}1_{TE/Ca\text{-}ratio} \times (57/168) + F\text{-}2_{TE/Ca\text{-}ratio} \times (75/168)$. For *N. dutertrei*, the sizes of the chambers in the final whorl are not very different and a weighted average based upon thickness is likely accurate. However, for *T. sacculifer*, the F chamber is the largest and thinnest chamber and the F-1 and F-2 chambers are generally similar in size but more thickly calcified, and so the weighted average might not be very accurate. We explore the implications of the nonweighted versus weighted averages in the discussion.

2.3. Solution ICP-MS Analysis

2.3.1. Sample Preparation for Solution ICP-MS

Following laser ablation analysis, foraminifera shells were removed from the carbon tape and then shipped to the INSTAAR Trace Metal Lab at the University of Colorado Boulder for analysis by solution ICP-MS, using methods described by Rongstad et al. (2017). Each shell was first weighed on a microbalance with 1 μg precision. Although the whole shells were previously cleaned for the LA analyses, remnant organic matter and fine clays can be present in the small inner chambers that were not exposed to cleaning. Specimens were therefore cracked open and oxidatively cleaned again prior to solution analysis. Individual shells were gently crushed between two glass microscope slides to open all chambers to cleaning reagents, then loaded into 500 μL polypropylene microcentrifuge vials that were preleached in hot 0.5 N HCl. The oxidative

Table 2
Orbulina universa Trace Element to Calcium Ratios Data

Specimen #	Laser Mg/Ca	Solution Mg/Ca	Laser Sr/Ca	Solution Sr/Ca
1	8.34	7.95	1.36	1.33
2	9.46	10.77	1.35	1.38
3	8.92	9.22	1.32	1.32
4	7.11	7.16	1.37	1.36
5	7.67	7.09	1.36	1.38
6	9.95	9.76	1.51	1.46
7	8.51	8.63	1.43	1.39
8	9.37	8.66	1.36	1.36
9	9.80	11.39	1.45	1.42
10	10.09	9.16	1.42	1.40
11	12.42	10.74	1.45	1.42
12	11.20	10.42	1.42	1.39
13	10.47	9.16	1.44	1.40
Mean	9.49	9.24	1.40	1.39
Std. dev (1σ)	1.44	1.36	0.06	0.04
Variance	2.07	1.85	0.003	0.002

cleaning procedure was developed from the methods of Boyle and Keigwin (1985/1986) and Barker et al. (2003), with several changes intended to minimize sample loss (Rongstad et al., 2017). Clays were siphoned away after each of four 1-min sonications alternating between methanol and ultrapure water. Samples were then heated for 10 min in 100 μL of an oxidative solution containing 0.4% of 30% H_2O_2 in 0.1 N NaOH, followed by five rinses in ultrapure water. Cleaned foraminifera were transferred to clean microcentrifuge vials and dissolved in 100 μL of 0.5% (0.075 N) trace metal grade HNO_3. Sample mass loss was estimated by comparing each sample's measured Ca concentration (in a known volume of acid) to its precleaning mass. The presence of infill prior to cleaning could lead to calculated sample losses being overestimated, but this effect is minimized by the precleaning prior to laser analysis.

2.3.2. Solution ICP-MS Protocol

Dissolved samples were pipetted into polytetrafluorethylene cups and diluted with 400 μL of 2% trace metal grade HNO_3 for analysis on a ThermoFinnigan Element2 magnetic sector ICP-MS, following the methods of Rongstad et al. (2017). Four external gravimetric liquid standards were brought to concentrations approximating those in samples containing 5 μg of $CaCO_3$, and were each analyzed four times during a run (between every eight samples). Five acid blanks were also analyzed during each run. To account for small sample sizes, dwell times (the amount of time spent measuring each discrete mass within an elemental peak scan) were increased relative to the routine trace metal method of Marchitto (2006): ^{26}Mg was increased tenfold to 0.1 s, and the contaminant indicators ^{27}Al, ^{55}Mn, and ^{56}Fe were doubled to 0.02 s. ^{43}Ca and ^{88}Sr remained at 0.01 s due to their relatively high count rates. All low-resolution isotopes (^{26}Mg, ^{43}Ca, ^{55}Mn, and ^{88}Sr) were run in Analog detection mode to ensure that metal/Ca ratios were measured in the same mode, while medium resolution isotopes (^{27}Al, ^{43}Ca, and ^{56}Fe) were run in both mode to accommodate a wide range of contaminant concentrations. Analysis of liquid consistency standards indicates analytical precision (±1σ) of 0.6% for Mg/Ca and 0.5% for Sr/Ca, with no significant dependence on sample size over the range of 0.2–100 μg $CaCO_3$ equivalent.

2.3.3. Solution ICP-MS Data Processing

Elemental ratios were calculated offline. Raw isotope count rates were first corrected for process and machine blanks by subtracting the linearly interpolated count rates of five acid blanks analyzed during each run. Blank-corrected TE counts were then ratioed to blank-corrected Ca counts, with those ratios in the four external standards being regressed against their known molar ratios to produce linear standard curves. Blank counts and standard curve slopes and intercepts were monitored for quality control. Sample molar ratios were then calculated using linear interpolation between the four standard curves, with one gravimetric liquid consistency standard being analyzed as an unknown for additional quality control. No resolvable matrix effects were observed over the small range of Ca concentrations investigated here.

3. Results

Average Mg/Ca and Sr/Ca ratios obtained for each specimen are detailed in Tables 2–5. For *O. universa* and *P. obliquiloculata*, we average repeat analyses to obtain whole shell specimen averages. For *T. sacculifer* and *N. dutertrei*, we report individual chamber ratios (averages of repeat spot analyses on the same chambers) and whole shell averages (individual chambers are averaged together). We report weighted and nonweighted averages for the multichambered species *T. sacculifer* and *N. dutertrei*.

Table 3
Pulleniatina obliquiloculata Trace Element to Calcium Ratios Data

Specimen #	Laser Mg/Ca	Solution Mg/Ca	Laser Sr/Ca	Solution Sr/Ca
1	3.64	3.36	1.37	1.39
2	2.64	2.54	1.39	1.38
3	2.49	2.56	1.48	**1.56**
4	3.88	3.73	1.42	1.45
5	2.80	2.16	1.52	1.43
6	2.33	2.39	1.38	1.37
7	3.30	3.32	1.41	1.42
8	2.86	2.71	1.37	1.37
9	3.71	3.11	1.55	1.45
10	3.28	3.39	1.36	1.42
11	2.40	1.83	1.49	1.47
12	3.04	2.62	1.39	1.42
13	2.24	2.00	1.36	1.37
14	2.91	3.07	1.45	1.44
15	2.49	2.46	1.34	1.39
Mean	2.93	2.75	1.42	1.42 (1.41)
Std. dev (1σ)	0.53	0.56	0.07	0.05 (0.03)
Variance	0.28	0.31	0.004	0.003 (0.001)

Notes. Bold font denotes a statistical outlier (>2σ). Values in () are calculated after excluding the outlier.

3.1. *O. universa*

3.1.1. Mg/Ca Data

LA-based Mg/Ca ratios range from 7.11 to 12.42 mmol/mol (mean: 9.49 ± 1.44 [1σ] mmol/mol; Figure 1a; Table 2). Solution-based Mg/Ca ratios range from 7.09 to 11.39 mmol/mol (mean: 9.24 ± 1.36 [1σ] mmol/mol; Figure 1a; Table 2). The two data sets have similar variances (Levene's test; $p = 0.95$) and the LA and solution-based Mg/Ca data are statistically (pairwise) similar (paired student's *t*-test, $p = 0.36$). The correlation between the two data sets, assessed using a Pearson's correlation coefficient, is 0.78 (Figure 2a).

3.1.2. Sr/Ca Data

LA-based Sr/Ca ratios range from 1.32 to 1.51 mmol/mol (mean: 1.40 ± 0.06 [1σ] mmol/mol; Figure 1b, Table 2). Solution-based Sr/Ca ratios range from 1.32 to 1.46 mmol/mol (mean: 1.39 ± 0.04 [1σ] mmol/mol; Figure 1b, Table 2). Variances between the two data sets are similar (Levene's test; $p = 0.09$). The LA and solution-based Sr/Ca data are not statistically similar (paired student's *t*-test, $p = 0.02$). The correlation between the two data sets, assessed using a Pearson's correlation coefficient, is 0.93 (Figure 2b).

3.2. *P. obliquiloculata*

3.2.1. Mg/Ca Data

LA-based Mg/Ca ratios range from 2.24 to 3.88 mmol/mol (mean: 2.93 ± 0.53 [1σ] mmol/mol; Figure 1c, Table 3). Solution-based Mg/Ca ratios range from 1.83 to 3.73 mmol/mol (mean: 2.74 ± 0.56 [1σ] mmol/mol; Figure 1c, Table 3). Variances between the two data sets are similar (Levene's test; $p = 0.77$). The LA and solution-based Mg/Ca data are not statistically similar (paired student's *t*-test, $p = 0.02$). The correlation between the two data sets, assessed using a Pearson's correlation coefficient, is 0.88 (Figure 3a).

3.2.2. Sr/Ca Data

LA-based Sr/Ca ratios range from 1.34 to 1.55 mmol/mol (mean: 1.42 ± 0.07 [1σ] mmol/mol; Figure 1d, Table 3). Solution-based Sr/Ca ratios range from 1.37 to 1.56 mmol/mol (mean: 1.42 ± 0.1 [1σ] mmol/mol; Figure 1d, Table 3). Variances between the two data sets are similar (Levene's test; $p = 0.18$). The LA and solution-based Sr/Ca data are statistically similar (paired student's *t*-test, $p = 0.89$). The correlation between the two data sets, assessed using a Pearson's correlation coefficient, is 0.65 (Figure 3b). There is one 2σ outlier in the Sr/Ca solution data (red box in Figure 3b). Removing the outlier increases the correlation coefficient to 0.74.

3.3. *T. sacculifer*

3.3.1. Mg/Ca Data

Nonweighted LA-based Mg/Ca ratios (see methods) range from 3.65 to 6.08 mmol/mol (mean: 4.46 ± 0.61 [1σ] mmol/mol; Figure 1e, Table 4). Weighted whole shell LA-based Mg/Ca ratios (see methods) range from 3.66 to 6.12 mmol/mol (mean: 4.50 ± 0.63 [1σ] mmol/mol; Figure 1e, Table 4). Individual chamber Mg/Ca means are 4.25 ± 0.77, 4.44 ± 0.63, and 4.70 ± 0.72 mmol/mol [1σ], for the F, F-1, and F-2 chambers, respectively (Figure 1e, Table 4). The F and F-1 chamber means are not significantly different (student's *t*-test,

Table 4
Trilobatus sacculifer Trace Element to Calcium Ratios Data

	Laser Mg/Ca data (mmol/mol)					Solution data (mmol/mol)	Laser Sr/Ca data (mmol/mol)					Solution data (mmol/mol)
	Chamber			Specimen mean			Chamber			Specimen mean		
Specimen #	F	F-1	F-2	Non-Wtd	Wtd	Mg/Ca	F	F-1	F-2	Non-Wtd	Wtd	
1	3.78	3.77	3.41	3.65	3.66	3.50	1.39	1.39	1.35	1.38	1.38	1.36
2	5.94	5.93	6.38	**6.08**	**6.12**	4.24	1.48	1.53	1.47	1.49	1.49	1.43
3	3.66	4.47	4.57	4.23	4.32	3.93	1.37	1.40	1.39	1.38	1.39	1.36
4	3.16	4.85	5.12	4.37	4.46	4.06	1.37	1.37	1.37	1.37	1.37	1.34
5	4.52	5.02	5.10	4.88	4.91	3.72	1.38	1.41	1.38	1.39	1.39	1.34
6	4.63	4.23	5.16	4.67	4.81	4.17	1.50	1.48	1.47	1.48	1.48	1.43
7	4.14	3.84	4.18	4.05	4.03	3.82	1.48	1.47	1.51	1.49	1.49	1.45
8	4.04	3.91	4.12	4.02	3.98	3.61	1.42	1.42	1.37	1.40	1.42	1.37
9	3.96	4.28	4.71	4.32	4.44	3.74	1.40	1.42	1.50	1.44	1.45	1.43
10	3.03	4.68	4.70	4.14	4.06	4.10	1.50	1.49	1.51	1.50	1.50	1.46
11	4.91	4.31	4.54	4.59	4.63	4.11	1.44	1.49	1.44	1.46	1.46	1.39
12	4.05	3.61	3.81	3.82	3.82	3.58	1.35	1.39	1.33	1.36	1.35	1.35
13	4.64	4.19	4.94	4.59	4.61	4.45	1.42	1.38	1.44	1.41	1.41	1.37
14	5.02	5.14	5.09	5.09	5.09	4.27	1.41	1.44	1.42	1.42	1.42	1.38
Mean	4.25	4.44	4.70	4.46	4.50	3.95	1.42	1.43	1.42	1.43	1.43	1.39
Std. dev 1σ	0.77	0.63	0.72	0.61	0.63	0.29	0.05	0.05	0.06	0.05	0.05	0.04
Variance	0.59	0.40	0.51	0.38	0.39	0.09	0.003	0.003	0.004	0.003	0.003	0.002

Note. Bold font denotes a statistical outlier (>2σ).

$p = 0.34$), however the F and F-1 chamber means are significantly different compared to the F-2 chamber (student's *t*-tests, $p = 0.03$ [F vs. F-2]; $p = 0.01$ [F-1 vs. F-2]). Solution-based Mg/Ca ratios range from 3.50 to 4.45 mmol/mol (mean: 3.95 ± 0.29 [1σ] mmol/mol; Figure 1e, Table 4). The whole shell LA-based Mg/Ca data (nonweighted and weighted sample means) are significantly higher than the solution-based data (paired student's *t*-tests, $p << 0.01$). Paired student's *t*-tests, to assess the similarity of individual chamber Mg/Ca data and the solution Mg/Ca data, show that the F chamber data are statistically similar to the solution data ($p = 0.13$), but the F-1 and F-2 data are not similar to the solution data ($p << 0.01$).

Variances between the F and F-1 data and the solution data are not similar (Levene's test; $p = 0.01$ and $p = 0.04$, respectively). The F-2 data and solution data variances are similar (Levene's test, $p = 0.06$). The variance of the mean LA-based Mg/Ca data (nonweighted and weighted) are similar to the solution data (Levene's test; $p = 0.10$ (nonweighted) and $p = 0.09$ (weighted)). When the outlier is excluded, the Levene's test for equal variances between the F, F-1, and F-2 chambers, the nonweighted and weighted mean LA data versus the solution data are as follows: $p = 0.03$, 0.12, 0.07, 0.27, and 0.13. That is, the variances of all but the F chamber are statistically similar to the variance of the solution data. The correlation between the LA-based data and the solution data, assessed using a Pearson's correlation coefficient, is 0.41, 0.54, 0.71, 0.64, and 0.63 for the F, F-1, F-2, nonweighted, and weighted data versus the solution data. When the outlier sample is removed, the correlation coefficients are 0.32, 0.50, 0.73, 0.67, and 0.66 for the F, F-1, F-2, nonweighted, and weighted LA data versus the solution data (Figures 4a–4e).

Table 5
Neogloboquadrina dutertrei Trace Element to Calcium Ratios Data

	Chamber						Specimen mean		Solution data
Specimen	F	F-1	F-2	F-3	F-4	F-5	Non-Wtd	Wtd	(mmol/mol)
				Laser Mg/Ca data (mmol/mol)					
1	4.24	3.21	2.94	2.78	3.03	3.18	3.23	3.09	
2	3.88	3.01	1.31	0.94	-	2.08	2.25	2.05	1.78
3	3.62	3.99	3.01	2.32	2.01	-	2.99	3.00	2.46
4	3.21	2.33	1.71	-	-	-	2.42	2.30	1.91
5	4.65	4.53	3.39	2.85	2.56	-	3.60	3.31	2.70
6	2.58	1.63	1.38	1.53	-	-	1.78	1.61	1.83
7	4.36	3.71	2.94	3.39	3.32	3.27	3.50	3.46	2.68
8	4.25	2.86	2.56	2.02	2.70	-	2.88	2.67	2.43
9	2.10	2.22	2.90	3.98	3.28	-	2.90	2.53	2.11
10	2.42	3.11	2.04	2.03	2.44	3.83	2.65	2.35	2.05
11	2.78	3.02	2.89	2.81	-	-	2.87	2.91	2.95
12	3.00	2.96	2.71	2.41	2.50	3.46	2.84	2.74	2.24
13	4.45	4.43	3.29	3.27	3.88	-	3.86	3.77	2.80
Mean	3.50	3.15	2.54	2.53	2.86	3.16	2.90	2.75	2.36
Std. dev (1σ)	0.87	0.85	0.70	0.84	0.57	0.65	0.57	0.60	0.40
Variance	0.75	0.71	0.49	-	-	-	0.32	0.36	0.16
				Laser Sr/Ca data (mmol/mol)					
1	1.53	1.43	1.37	1.31	1.37	1.41	1.40	1.38	1.39
2	1.46	1.44	1.40	1.50	-	1.42	1.44	1.44	1.42
3	1.49	1.51	1.45	1.46	1.47	-	1.48	1.47	1.43
4	1.31	1.31	1.34	-	-	-	1.32	1.32	1.35
5	1.38	1.44	1.35	1.30	1.36	-	1.37	1.36	1.44
6	1.38	1.33	1.38	1.39	-	-	1.37	1.36	1.37
7	1.41	1.33	1.35	1.28	1.34	1.40	1.35	1.33	1.40
8	1.34	1.33	1.25	1.34	1.31	-	1.31	1.32	1.34
9	1.38	1.32	1.38	1.43	1.43	-	1.39	1.38	1.36
10	1.43	1.43	1.43	1.43	1.45	1.44	1.43	1.43	1.43
11	1.39	1.37	1.30	1.37	-	-	1.36	1.34	1.33
12	1.46	1.40	1.30	1.35	1.37	1.34	1.37	1.36	1.41
13	1.42	1.47	1.47	1.45	1.38	-	1.44	1.44	1.42
Mean	1.41	1.39	1.37	1.38	1.38	1.40	1.39	1.38	1.39
Std. dev (1σ)	0.06	0.07	0.06	0.07	0.05	0.04	0.05	0.05	0.04
Variance	0.004	0.004	0.004	-	-	-	0.003	0.003	0.002

3.3.2. Sr/Ca Data

LA-based Sr/Ca ratios range from 1.36 to 1.50 mmol/mol (mean: 1.43 ± 0.05 [1σ] mmol/mol; Figure 1f, Table 4). F, F-1, and F-2 Mg/Ca chamber means are 1.42 ± 0.05, 1.43 ± 0.05, and 1.42 ± 0.06 mmol/mol [1σ], respectively. The F-1 chamber is statistically different from the F and F-2 chambers (student's *t*-test, $p = 0.01$ and $p = 0.02$ for the F vs. F-1 and F-1 vs. F-2, respectively), however the F-1 and F-2 chamber means are not significantly different (student's *t*-tests, $p = 0.70$). Solution-based Sr/Ca ratios range from 1.34 to 1.46 mmol/mol (mean: 1.39 ± 0.04 [1σ] mmol/mol; Figure 1f, Table 4). The LA-based Sr/Ca data

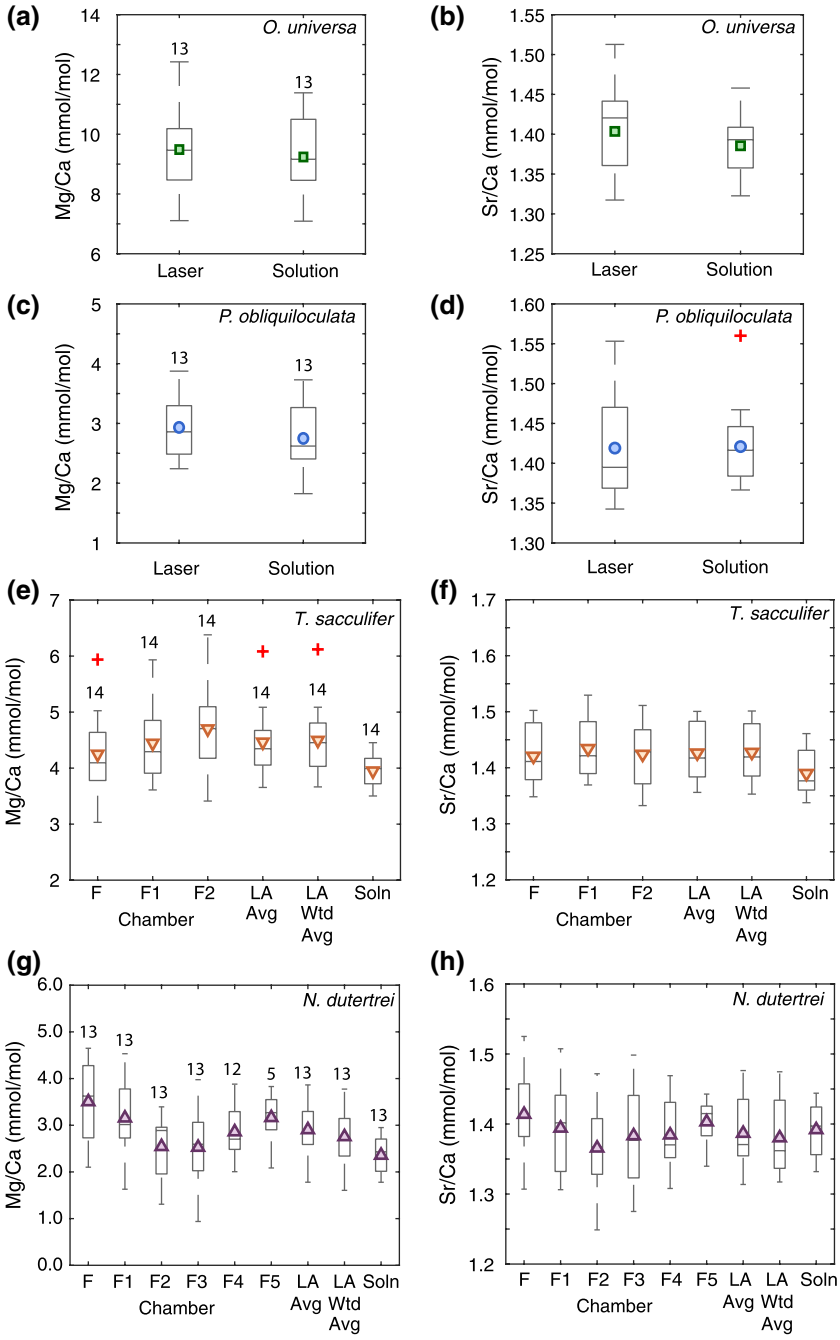

Figure 1. Boxplots of the Mg/Ca (a, c, e, and g) and Sr/Ca (b, d, f, and h) data for *Orbulina universa* (a and b), *Pulleniatina obliquiloculata* (c and d), *Neogloboquadrina dutertrei* (e and f) and *Trilobatus sacculifer* (g and h). Colored triangles within each boxplot are the mean trace element to calcium ratios. Numbers above boxes refer to the number of chambers/analyses represented by the box plots. Red "plus" symbols denote statistical outliers (>2σ).

(whole shell nonweighted and weighted data) are not statistically similar to the solution-based data (paired student's *t*-tests, $p << 0.01$).

Variances between the F and F-1 chambers and the solution data are not similar (Levene's test; $p = 0.01$ and $p = 0.04$, respectively). Variances between the F-2 and solution data are similar (Levene's test, $p = 0.06$). The variance of the mean LA based data (nonweighted and weighted) are similar to the solution data (Levene's test; $p = 0.10$ [nonweighted] and $p = 0.09$ [weighted]). The correlation between the LA-based Sr/Ca

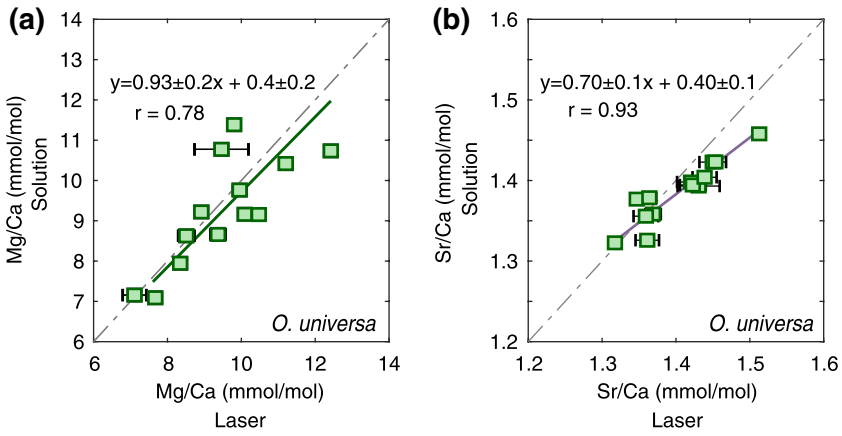

Figure 2. Scatter plots of the (a) Mg/Ca and (b) Sr/Ca data from the *Orbulina universa* paired laser (*x*-axis) and solution analyses (*y*-axis). The dashed line in each plot is the 1:1 line. The solid line represents the slope of a type 2 regression analysis. The *r* value is the correlation coefficient. The error bars are the standard deviation of repeat analyses on the same specimen.

data and the solution Sr/Ca data, assessed using a Pearson's correlation coefficient, is 0.87, 0.79, 0.91, 0.93, and 0.95 for the F, F-1, F-2, mean nonweighted and weighted data versus the solution data, respectively (Figures 4f–4j).

3.4. *N. dutertrei*

3.4.1. Mg/Ca Data

Nonweighted LA-based Mg/Ca ratios (see methods) range from 1.78 to 3.86 mmol/mol (mean: 2.90 ± 0.57 [1σ] mmol/mol; Figure 1g, Table 5). Weighted whole shell LA-based Mg/Ca ratios (see methods) range from 1.61 to 3.77 mmol/mol (mean: 2.75 ± 0.60 [1σ] mmol/mol; Figure 1g). Individual chamber Mg/Ca means are 3.50 ± 0.87, 3.15 ± 0.85, 2.54 ± 0.70, 2.53 ± 0.84, 2.86 ± 0.57, and 3.16 ± 0.65 (1σ) mmol/mol, for the F, F-1, F-2, F-3, F-4, and F-5 chambers, respectively (Figure 1g, Table 5). Note that the F-4 chamber was analyzed in nine specimens and the F-5 chamber was analyzed in only five of the 13 specimens (Table 5). Chamber means are statistically different (Kruskal-Wallis Analysis of Variance (ANOVA): Chi-squared 11.5, $p = 0.04$). Solution-based Mg/Ca ratios range from 1.78 to 2.95 mmol/mol (mean: 2.36 ± 0.40 [1σ] mmol/mol; Figure 1g, Table 5). The mean LA-based Mg/Ca data are not statistically similar to the solution-based

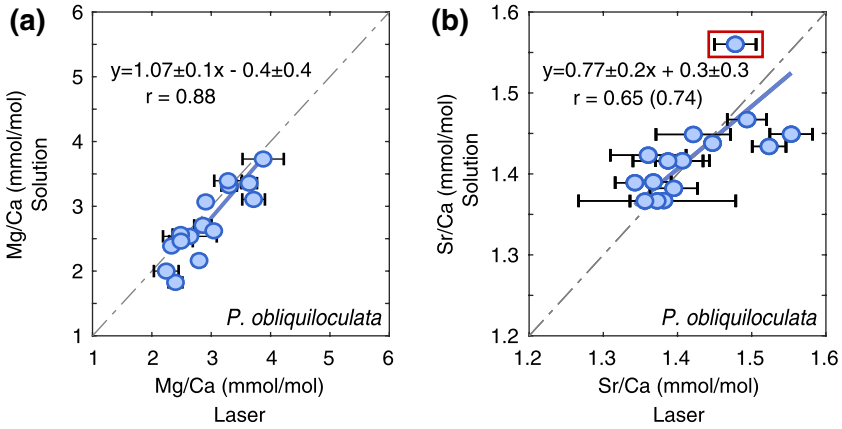

Figure 3. Scatter plots of the (a) Mg/Ca and (b) Sr/Ca data from the *Pulleniatina obliquiloculata* laser (*x*-axis) and solution analyses (*y*-axis). The dashed and solid lines and error bars in each plot are the same as in Figure 2. The *r* value is the correlation coefficient (*r* value in parenthesis is the correlation coefficient after excluding the statistical outlier [red box]).

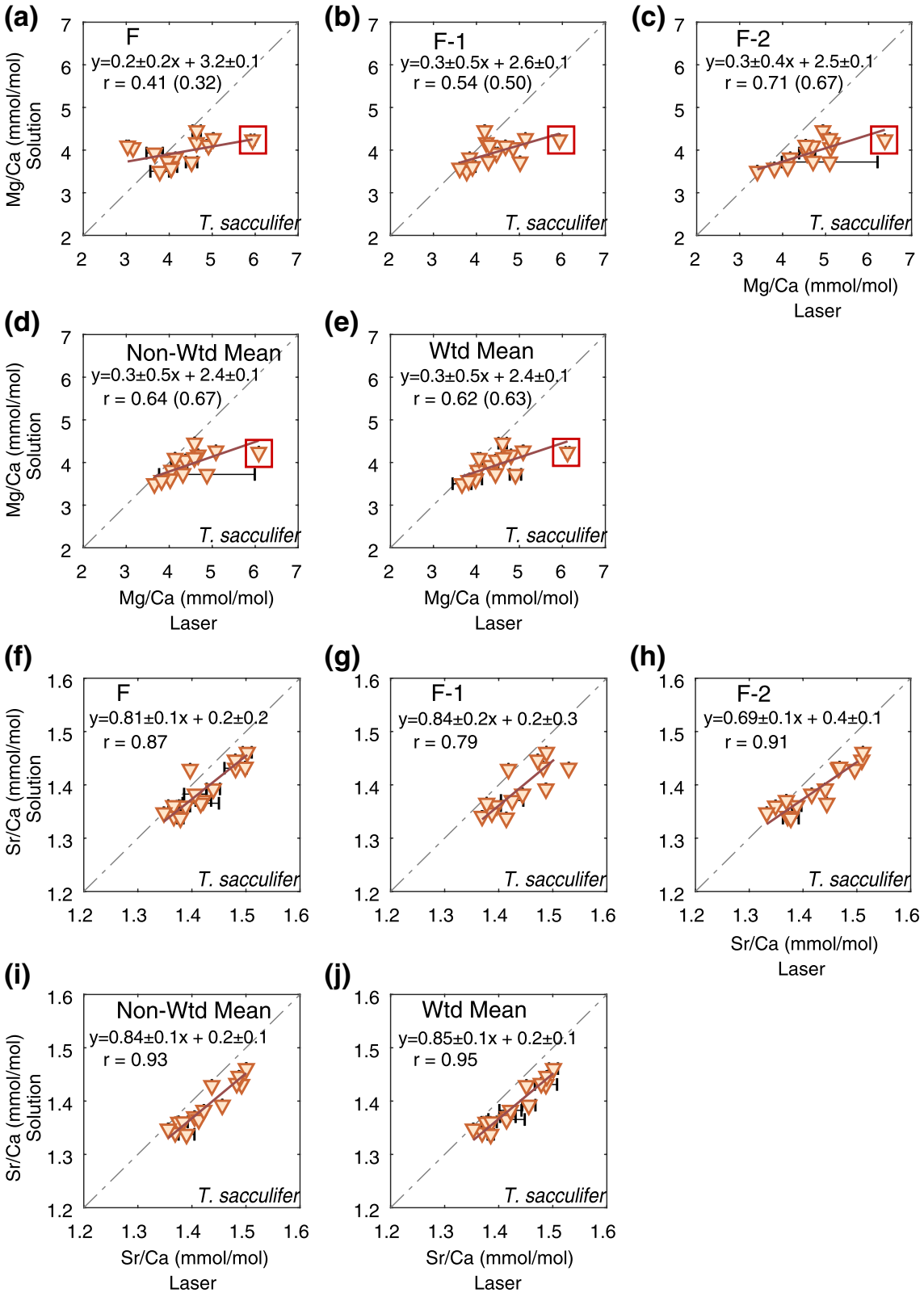

Figure 4. Scatter plots of the Mg/Ca (a–e) and Sr/Ca (f–j) data from *Trilobatus sacculifer* paired laser (*x*-axis) and solution analyses (*y*-axis). Mg/Ca data for individual chambers (a–c), nonweighted (d), and weighted means (e) versus solution data. Sr/Ca data for individual chambers (f–h), nonweighted (i), and weighted (j) means. Dashed and solid lines are similar to Figure 2 The *r* value is the correlation coefficient (*r* value in parenthesis is the correlation coefficient after excluding the statistical outlier (red box in [a–e]).

data (paired student's *t*-test, $p << 0.01$ for both nonweighted and weighted LA data vs. solution data). Paired student's *t*-tests, to assess the similarity of the mean Mg/Ca ratios of individual chambers and the solution data, show that the F and F-1 chamber means are not similar to the mean of the solution data ($p << 0.01$). The F-2, F-3, and F-4 chamber means are similar to the mean of the solution data ($p = 0.13$, 0.51, and 0.50, for the F-2, F-3, and F-4 chambers, respectively).

Variances between the whole shell LA data and the solution data sets are similar whether the LA sample means are nonweighted (Levene's test; $p = 0.58$) or weighted (Levene's test; $p = 0.27$). A Levene's test for homogeneity of variance reveals the F and F-2 chambers do not have similar variance when compared to the solution data, but the F-1, F-3, and F-4 chambers have similar variance compared to the solution data. The correlation between the solution data and the F, F-1, F-2, F-3, F-4, whole shell nonweighted, and whole shell weighted data, assessed using a Pearson's correlation coefficient, is 0.51, 0.68, 0.86, 0.60, 0.41, 0.82, and 0.88, respectively (Figures 5a–5g).

3.4.2. Sr/Ca Data

LA-based Sr/Ca ratios range from 1.31 to 1.48 mmol/mol (mean: 1.39 ± 0.05 [1σ] mmol/mol; Figure 1h, Table 5). Weighted whole shell Sr/Ca ratios (see methods) range 1.31–1.47 mmol/mol (mean: 1.38 ± 0.05 mmol/mol [Figure 3a]. The F, F-1, F-2, F-3, and F-4 chamber Sr/Ca means are 1.41 ± 0.06, 1.39 ± 0.07, 1.37 ± 0.06, 1.38 ± 0.07, and 1.38 ± 0.05 (1σ), respectively (Table 5). Chamber means are statistically similar (Kruskal-Wallis ANOVA: Chi-squared 3.5, $p < 0.57$). Solution-based Sr/Ca ratios range from 1.33 to 1.44 mmol/mol (mean: 1.39 ± 0.04 [1σ] mmol/mol [Figure 1h]). Nonweighted and weighted LA-based Sr/Ca data are statistically similar to the solution-based data (paired student's *t*-test, $p = 0.62$ and $p = 0.29$ for the LA-based nonweighted and weighted data, respectively). Paired student's *t*-tests, to assess the similarity of the mean Sr/Ca ratios of individual chambers and the solution data, show that the Sr/Ca ratios of all individual chambers are similar to the solution data ($p = 0.13$, 0.85, 0.07, 0.58, and 0.28 for the F, F-1, F-2, F-3, and F-4 chambers, respectively

Variances between the F-1 and F-3 chambers are not similar to the variance of the solution data, however the F, F-2, and F-4 chamber variances are similar to the variance of the solution data. Variances between the whole shell LA data and the solution data sets are similar whether the LA sample means are nonweighted (Levene's test; $p = 0.41$) or weighted (Levene's test; $p = 0.37$). The correlation, assessed using a Pearson's correlation coefficient, between the solution data and the F, F-1, F-2, F-3, F-4, whole shell nonweighted LA data, and whole shell weighted data is 0.59, 0.80, 0.64, 0.21, 0.44, 0.69, and 0.88, respectively (Figures 5h–5n).

4. Discussion

Ideally, TE/Ca ratios measured on the same foraminifer specimen would be in agreement regardless of how the analyses are performed. Here, we show that Mg/Ca and Sr/Ca ratios compare well when the same specimens are analyzed on a laser and then subsequently in solution (Figure 6). For foraminifers of simple morphology, like *O. universa*, and heavily calcified *P. obliquiloculata* with thick cortexes, the data from either technique are generally within instrument error, are moderately to highly correlated, and have similar variances (Figures 1a–1d, 2, and 3). For foraminifers with more complex morphologies, like *N. dutertrei* and *T. sacculifer*, the correlation between the two techniques is highest when all chambers in the final whorl of the shell are analyzed on the laser and the specimen averages are weighted (Figures 4 and 5). However, the laser values for these two species still tend to be slightly higher than the solution values and the slopes between the two techniques are often far from a 1:1 relationship. The greatest disagreement between the two techniques arises when single chamber LA-ICP-MS TE data are compared to the solution data from an entire shell. For example, for *T. sacculifer*, the Mg/Ca data for the F and F-1 chambers are only moderately correlated with the solution data ($r = 0.41$ and 0.54, for the F and F-1 chambers respectively; Figures 4a and 4b), but the correlation increases if the laser data from all chambers is averaged ($r = 0.64$ and 0.62 for nonweighted and weighted means, respectively; Figure 4e). For the same specimens, the Sr/Ca data is highly correlated with the solution data regardless of which individual chamber is analyzed and the correlation only slightly improves when the whole shell averages are weighted ($r = 0.95$) (Figures 4F–4j). For *N. dutertrei*, the Mg/Ca and Sr/Ca laser data for different chambers is far more variable than the solution data and correlations improve considerably ($r = \sim 0.9$) when the specimen averages are weighted (Figure 5). For

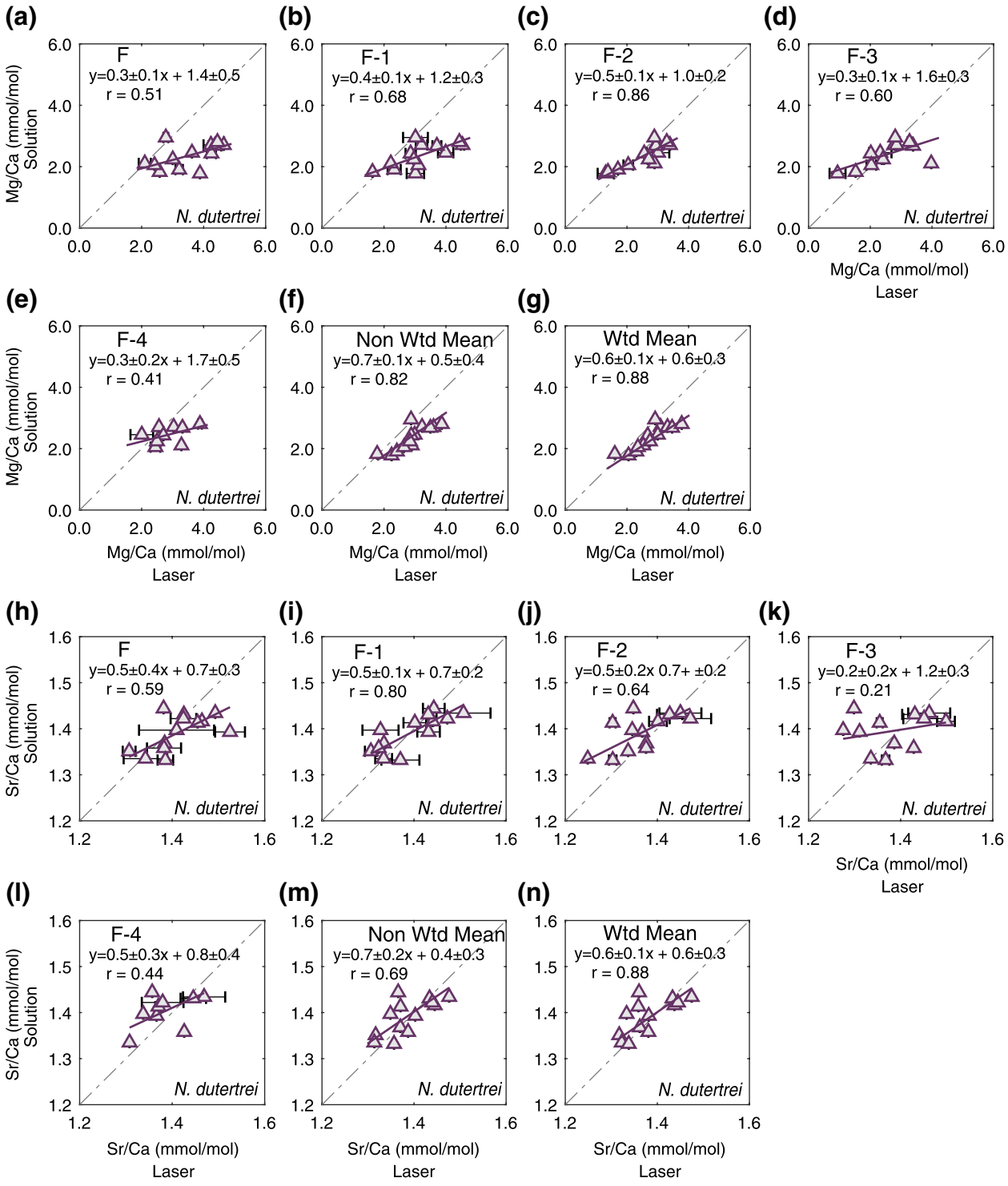

Figure 5. Scatter plots of the Mg/Ca (a–g) and Sr/Ca (h–n) data from the *Neogloboquadrina dutertrei* paired laser (*x*-axis) and solution analyses (*y*-axis). Mg/Ca data for individual chambers (a–e), nonweighted (f), and weighted (g) means versus solution data. Sr/Ca data for individual chambers (h–n), nonweighted (m), and weighted (n) means. Dashed and solid lines in each plot as in Figure 2.

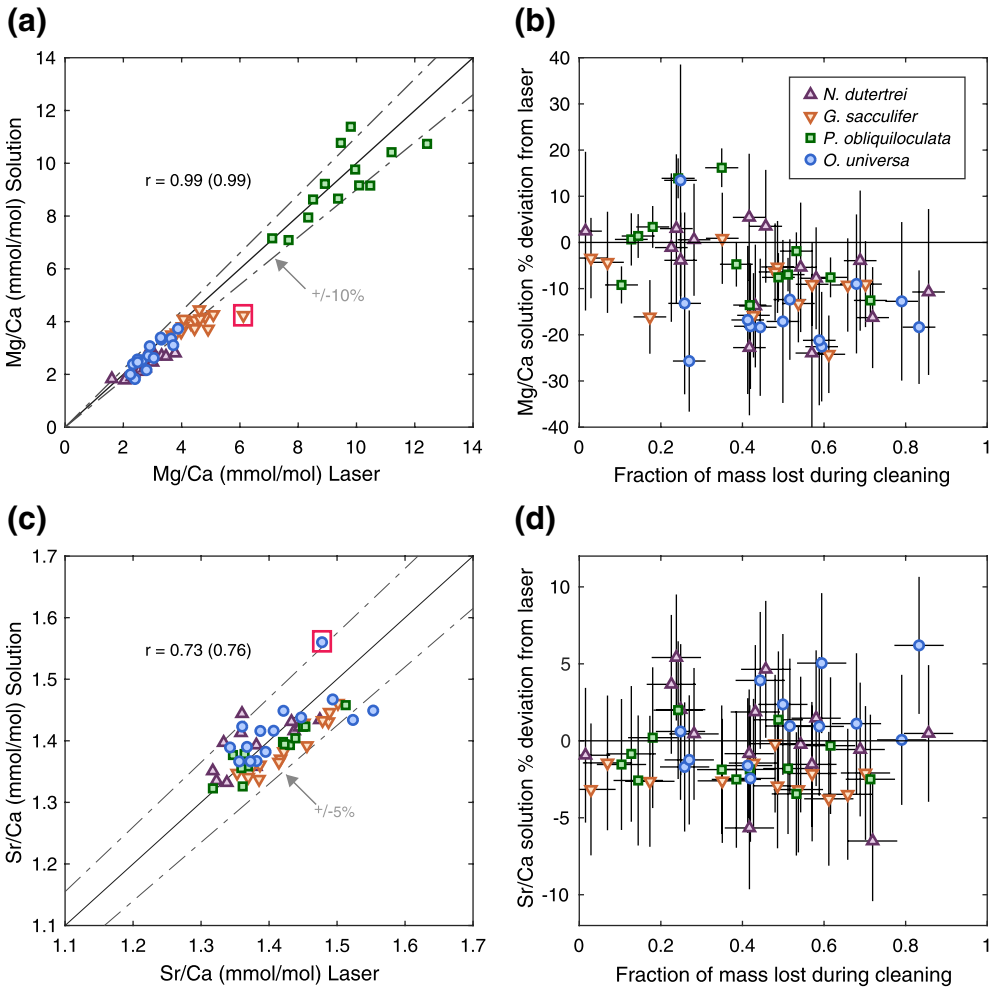

Figure 6. (a) Mg/Ca and (c) Sr/Ca data for all specimens analyzed via LA-ICP-MS (weighted means) and solution-based ICP-MS. The solid line represents a 1:1 correlation between the two techniques. The gray dashed lines represent the ± 10% and ± 5% 1:1 correlation for the Mg/Ca and Sr/Ca data, respectively. The *r* value is the Pearson's correlation coefficient. The *r* values in parentheses are the correlation coefficients after removing outliers (red boxes). (b) Mg/Ca and (d) Sr/Ca solution percentage deviation from the laser data versus the fraction of shell mass lost during cleaning for the solution-based analyses. ICP-MS, Inductively coupled plasma-mass spectrometry.

both species, the variance is highest among F chambers and decreases with ontogenic age (older chambers have lower variance). The variance of the laser data is most similar to the solution data variance when the laser data is averaged for all chambers. These results suggest that for multichambered species, especially those with significant chamber-to-chamber TE variability (Figures 1e–1h), all chambers in the final whorl should be analyzed when using the laser, especially if results (population means and/or variances) are to be used to compute the average environmental conditions experienced by an individual and/or compared to interpretations that rely on solution-based IFA.

In the discussion below, we first explore possible mechanisms that could explain offsets in the average TE/Ca values between the two techniques. We then explore assumptions made when interpreting single chamber TE/Ca data derived from the laser and offer best practices for generating and interpreting IFA TE data.

4.1. Possible Sources of TE/Ca Offsets

The two IFA methods compared in this study are not intercalibrated methods. The general agreement between the TE/Ca ratios measured in the species with simple morphology or crusts (*O. universa* and *P. obliquiloculata*) and the generally better correlation between Sr/Ca data compared to the Mg/Ca data

suggests that the offsets in the TE/Ca values in the species of more complex morphologies is not analytical. And, the overall agreement between the two techniques, especially when all chambers in the final whorl of multichambered species are analyzed, is quite good. Here, we explore potential mechanisms that could be responsible for an offset in the TE/Ca ratios between the two techniques.

4.1.1. Exclusion of Earliest (Juvenile) Chambers and Septa Calcite With LA-ICP-MS

LA-ICP-MS targets specific chambers in a shell, typically the largest chambers in the final whorl, and also typically excludes the earliest (and smallest) "juvenile" chambers. For a species like *T. sacculifer*, these smallest chambers can account for 10%–15% of the calcite in a shell (Spero & Lea, 1993). The calcite internal to the shell, for instance the septa between chambers and interior chambers (Brummer et al., 1986, 1987), which could have different trace element compositions, are also excluded during LA-ICP-MS analyses. If the small chambers and internal calcite have lower TE/Ca ratios, this could partially explain the sometimes higher TE/Ca ratios of the LA-ICP-MS results compared to the whole shell solution analyses. However, the large chambers of the final whorl comprise most of the shell calcite and juvenile chambers and inner calcite walls are relatively thin (Johnstone et al., 2010). Thus, we assume that if juvenile and inner calcite portions of the shell do have different TE composition compared to the calcite that forms the final whorl, they do not contribute enough mass to the final shell weight to explain differences between laser and whole shell solution analyses. It is also possible that thin septal calcite and inner chambers are preferentially lost during the chemical cleaning process required for solution-based analyses. If correct, then both methods would yield data that is derived primarily from the chambers in the final whorl.

4.1.2. Loss of Early Ontogenic (Lamellar) Calcite During Cleaning for Solution Analysis

The multistep cleaning process for the solution-based IFA, which requires gently cracking the shells into fragments followed by sonication rinses and an oxidative step (see Methods), decreases the sample mass (Figures 6b and 6d). The mass loss does not cause an appreciable offset in the Sr/Ca ratios (Figure 6d), but does yield a greater method offset for Mg/Ca ratios. Solution-based Mg/Ca is consistently lower than laser when mass loss exceeds ~40%–50%, particularly for *N. dutertrei*, *P. obliquiloculata*, and *O. universa* (Figure 6b). A possible explanation could be the preferential removal of the shell wall that has higher Mg/Ca ratios during the physical (sonication) and chemical (oxidative) cleaning process required for solution-based analyses.

The early ontogenic calcite that forms the inner calcite in final whorl chambers in deeper dwelling foraminifera, like *N. dutertrei* and *P. obliquiloculata*, has a microcrystalline texture compared to the outer calcite that forms during later ontogeny (i.e., see Figure 4 in Hathorne et al., 2009). When the shells are cracked for cleaning, it is possible that the microcrystalline inner calcite breaks into smaller fragments. The shells are also sonicated during rinse and oxidation steps, which can further fragment the microcrystalline inner calcite portions of the shell. These smaller fragments are more likely to be aspirated during cleaning or possibly even dissolve completely. Because the inner calcite is enriched in trace elements such as Mg, Ba, and Mn compared to the crust (Jonkers et al., 2012; Steinhardt et al., 2015), this process would preferentially leave the robust, and trace element poor, crust/cortex behind. Preferential removal of the microcrystalline calcite would not affect Sr/Ca or other TEs that are homogeneous throughout the shell wall.

O. universa also has a slightly lower Mg/Ca ratio when greater than ~40%–50% of the shell is removed during solution cleaning. The wide range of sample loss is likely dominated by fragmentation and aspiration, but dissolution could play a role. Although the oxidative step should be minimally corrosive to calcite, any dissolution that occurs during cleaning likely removes the exterior (exposed) calcite from the inner and outer shell wall (Sadekov, 2010; Vetter, 2013). Because Mg/Ca banding in this species is lowest near the primary organic sheet and increases as the shell thickens, removal of the outermost calcite from both the interior and exterior shell walls could therefore decrease the overall Mg/Ca ratios due to preferential removal of the outermost, and highest, Mg/Ca band (Spero et al., 2015). It is also possible that the inner calcite layer, which is very thin compared to the calcite that grows outward from the primary organic membrane, could fragment into smaller pieces during the cleaning process due to preferential fragmentation of this thin calcite layer. Again, these processes would only affect Mg/Ca ratios because Sr/Ca ratios are nearly constant throughout the shell wall of this species.

4.2. Implications for Paleoceanographic Reconstructions

Since Emiliani published the first paleoceanographic study on foraminifera isotope geochemistry (Emiliani, 1955), the research community has explored large-scale changes in mean ocean chemistry and paleoclimate throughout the Cenozoic and beyond. Despite this rich literature, few studies have probed the archive of paleoenvironmental information contained within foraminifera populations. IFA make it possible to study this population geochemistry and explore the environmental and ecological information contained within fossil foraminifera assemblages. One of the most exciting advances is the expanding use of different geochemical instruments on the same foraminifera shells to obtain linked environmental information (e.g., TE and isotope data; Vetter et al., 2017). However, interpreting IFA data requires the *a priori* assumption that the sample mean from analyses of numerous fossil shells together, and population variability from averages of multiple IFA, is not impacted by the analytical methods used. The fidelity of the results obtained and ability to cross-compare paleoceanographic reconstructions from IFA using different analytical techniques also relies on this assumption. Here, we explore the implications of using different analytical techniques to generate TE data for paleoceanographic reconstructions.

4.2.1. Species With Simple Morphology or Minimal Chamber-to-Chamber Variability

For *O. universa* and *P. obliquiloculata*, the Mg/Ca and Sr/Ca data derived from both laser- and solution-based analyses yields similar means and variances (Tables 2 and 3). Although the Sr/Ca data for *P. obliquiloculata* are not statistically (pairwise) similar, the population means and standard deviations are nearly identical and the two sets of data have similar variances, thus interpretations derived from either data set, if used in a paleoceanographic reconstruction, would be the same. We infer from these results that either analytical technique could be used for *O. universa* and species that are heavily calcified with a crust or cortex that dominates the shell calcite. Other species that likely make good candidates for using either technique would include, for example, heavily calcified specimens from the *Neogloboquadrinid* and *Globorotalid* genera. For such specimens, laser spot analyses would be dominated by the crust or cortex regardless of the location on the shell that the analyses were obtained. Because the solution analyses would also be composed of mostly crust/cortex calcite, the results obtained from either technique would likely be similar, as demonstrated by the *P. obliquiloculata* data presented here. Similarly, heavily calcified specimens from the seafloor that have undergone dissolution, and thus are missing the interior heterogeneous lamellar calcite surfaces (e.g., Johnstone et al., 2010), would likely yield similar TE/Ca data using either technique because the analyses would be dominated by the crust or cortex calcite. Studies have demonstrated that some heavily calcified species have minimal chamber-to-chamber variability, which means that they are good candidates for LA analyses where only the select chambers in the final whorl can be analyzed without introducing potential bias in the results (e.g., Reynolds et al., 2018).

4.2.2. Morphologically Complex Species and Those With High Chamber-To-Chamber Variability

Multichambered foraminifera have morphologically complex shells with a variable number of chambers in the final whorl. Many species also exhibit high chamber-to-chamber trace element variability (Bolton & Marr, 2013; Hathorne et al., 2009; Jonkers et al., 2012; Wit et al., 2010). The *N. dutertrei* data presented demonstrates high chamber-to-chamber variability, confirming the findings of Jonkers et al. (2012) who also demonstrated that the Mg/Ca ratio of *N. dutertrei* increases through ontogeny. For *N. dutertrei*, the F chamber typically has the highest Mg/Ca ratio, which decreases as the chambers become ontogenically older. We demonstrate that *T. sacculifer* also has high chamber-to-chamber variability, but this appears to be specific to geographic location. For example, Fritz-Endres et al. (2019) found minimal chamber-to-chamber variability in *T. sacculifer* specimens obtained from core-top samples in the Indian Ocean.

For species with demonstrated chamber-to-chamber variability, the method for obtaining trace element IFA data could impact paleoceanographic interpretations if whole shell ratios are the target of a study. The TE/Ca ratios obtained from individual chambers or a subset of chambers may not yield a similar TE/Ca data when analyzed via different techniques. For example, the F chamber of the *N. dutertrei* specimens analyzed in this study have a mean Mg/Ca ratio of 3.5 mmol/mol. By comparison, the solution data yields a much lower Mg/Ca ratio of 2.36 mmol/mol. If this data were used to generate downcore paleotemperatures, one would obtain a calcification temperature 4.4°C cooler using the solution-based ratio (temperatures difference calculated by using Anand et al., 2003 multispecies calibration).

Of additional importance is the difference in the population geochemical variability (e.g., the population variance), which is often interpreted in terms of interannual variability, seasonality, or depth habitat differences among individuals in a population of specimens at the time of calcification (e.g., Ford et al., 2015; Rongstad et al., 2020) or as an assessment of postdepositional alteration (Rongstad et al., 2017). Here, we demonstrate that variance differs from chamber-to-chamber within the same morphologically complex species and, at least for the Mg/Ca data, is generally not similar when comparing laser versus solution data. Differences between the laser and solution variances are also dependent on the chamber analyzed. In general, the variance is higher for the laser-based Mg/Ca data, especially when only individual chambers are considered. For example, the F chamber Mg/Ca laser data for *N. dutertrei* has a variance of 0.75 mmol/mol compared to 0.40 mmol/mol for the solution data. The laser variance decreases to 0.60 mmol/mol when all of the chambers are combined for a specimen average. Potential issues would therefore arise when comparing two studies that used different analytical methods to assess population variance. The interpretation of Mg/Ca data from a single study would be impacted less by this issue, because all of the specimens would be analyzed using the same technique.

If one were to interpret the range of Mg/Ca-derived temperature data as an indicator of species seasonality or depth habitat range, the solution versus laser-based results could yield markedly different results. For *N. dutertrei*, the range in temperatures (SSTs) derived from either the F-chamber only or the weighted mean data yield an 8.3°C difference in calcification temperatures. The solution data, by comparison, yield a SST range of 5.6°C. As a thermocline dweller, either range could be reasonably interpreted to reflect the species depth habitat range. For *T. sacculifer*, the F-chamber derived SSTs span 7.5°C and the specimen weighted average SSTs span only 3.7°C. By comparison, the solution data yields a smaller SST range of 2.8°C. Given that *T. sacculifer* occupies a mixed-layer depth habitat, it is highly unlikely that the temperature range indicated by the F-chamber data are realistic for the western equatorial Pacific location of our samples unless some individuals in our analyses were calcifying in the thermocline or were bioturbated glacial specimens. Rather, it is more likely that the chamber-based laser data is capturing the variable biological signature related to Mg banding within chambers that overprints the primary environmental signal. Sadekov et al (2008) called this nontemperature variability at the IFA level "stochastic biological variability." For the species *G. ruber*, they estimated the nontemperature related Mg/Ca variability to be equivalent to 1.6°C. Even in morphologically simple foraminifera species like *O. universa*, there is a considerable amount of nontemperature-related TE variability, likely linked to the number of days the spherical chamber calcified (Spero et al., 2015). Whereas the observed correlations between single chamber and whole shell Mg/Ca data clearly demonstrate that temperature information is preserved at the chamber level, the results indicate that weighted laser IFA data from multiple chambers yields more consistent environmental information then laser data from single chamber IFA. Perhaps more important, these results demonstrate that Mg/Ca data from an individual chamber (e.g., F chamber) should not be used for paleotemperature reconstructions, nor should chamber-to-chamber Mg/Ca data be used to reconstruct the vertical water column migration history of an individual foraminifera because of the significant stochastic biological variability overprint on each chamber.

As noted above, difficulties in interpreting and comparing paleoceanographic reconstructions that utilize IFA arise when comparing reconstructions from studies that utilize different analytical techniques. These findings highlight the need to establish community-wide protocols for IFA techniques that would minimize such issues. For example, results presented here suggest for multichambered species with high chamber-to-chamber TE variability, all chambers in the final whorl should be analyzed using LA-ICP-MS in order to minimize differences with data derived from solution-based IFA. This is particularly true if results are to be compared to solution-based analyses, for which sample loss should be assessed. Nevertheless, depending on the species being studied or the questions being asked, single chamber analyses by LA-ICP-MS (especially when used in conjunction with IRMS analyses) can still play an important role in probing fundamental paleoceanographic questions as long as the issues discussed in this study are considered.

5. Conclusion

Studies utilizing geochemical tools to study individual foraminifer shells from fossil populations is a rapidly expanding research area in paleoceanography. Interpretation of IFA data depends on the assumption that the data generated are not impacted by the analytical technique used in a study. Here we demonstrate that

laser-based TE/Ca ratios on foraminifera shells compare moderately well with data from solution-based techniques. This is especially true for foraminifera with simple morphologies such as *O. universa* or heavily calcified specimens with homogeneous TE geochemistry in the outer calcite crust such as *P. obliquiloculata*. Analyses of numerous chambers in the final whorl of multichambered species *N. dutertrei* and *T. sacculifer* yield comparable results to solution analyses when whole shell averages (weighted by chamber contribution to the mean) are calculated (Figure 6).

We highlight potential issues interpreting and comparing studies that use different analytical techniques and recommend that the paleoceanographic community establish accepted protocols for generating IFA that would permit cross-study comparisons between paleoceanographic reconstructions that utilize different analytical techniques: (1) we recommend when using LA-ICP-MS, all chambers in the final whorl should be analyzed and whole shell average TE/Ca ratios should be calculated using a weighted mean approach; (2) we recommend adopting careful cleaning procedures for solution analysis to minimize and monitor sample loss, in particular taking care to minimize loss of inner calcite; (3) we discourage the use of single chamber LA-ICP-MS-based analyses for temperature reconstructions, even if chamber specific temperature calibration equations are utilized, because of the significant and variable stochastic biological overprint on individual chambers in a shell.

Data Availability Statement

The raw laser ablation data associated with this manuscript (including Ca, Mg, Sr, and Al data) and the LA-Tools data processing commands are available at: DOI:10.5281/zenodo.4265147.

Acknowledgments
The authors thank reviewers J. Hertzberg and L. Jonkers who improved an earlier version of this manuscript. Jennifer Fehrenbacher prepped the samples for and analyzed the specimens by laser. Thomas Marchitto cleaned and analyzed the specimens in solution. Thomas Marchitto was supported by NSF grant OCE-1603023. Howard J. Spero was supported by NSF grants OCE-0550703 and EAR-0946297. Jennifer Fehrenbacher was supported by NSF grant OCE-1261519. All authors contributed to interpreting the data. Jennifer Fehrenbacher wrote the manuscript with significant contribution from all authors.

References

Allen, K. A., Honisch, B., Eggins, S. M., Haynes, L. L., Rosenthal, Y., & Yu, J. M. (2016). Trace element proxies for surface ocean conditions: A synthesis of culture calibrations with planktic foraminifera. *Geochimica et Cosmochimica Acta*, *193*, 197–221.

Anand, P., Elderfield, H., & Conte, M. H. (2003). Calibration of Mg/Ca thermometry in planktonic foraminifera from a sediment trap time series. *Paleoceanography*, *18*(2), https://doi.org/10.1029/2002PA000846

Babila, T. L., Penman, D. E., Honisch, B., Kelly, D. C., Bralower, T. J., Rosenthal, Y., & Zachos, J. C. (2018). Capturing the global signature of surface ocean acidification during the Palaeocene-Eocene Thermal Maximum. *Philosophical Transactions of The Royal Society A Mathematical Physical and Engineering Sciences*, *376*(2130). http://dx.doi.org/10.1098/rsta.2017.0072

Barker S., Greaves M., Elderfield H. (2003). A study of cleaning procedures used for foraminiferal Mg/Ca paleothermometry. *Geochemistry, Geophysics, Geosystems*, *4*(9). https://doi.org/10.1029/2003gc000559

Be, A. W. H., Hemleben, C., Anderson, O. R., Spindler, M., Hacunda, J., & Tuntivate-Choy, S. (1977). Laboratory and field observations of living foraminifera. *Micropaleontology (New York)*, *23*(2), 155–179.

Billups, K., & Spero, H. J. (1996). Reconstructing the stable isotope geochemistry and paleotemperatures of the equatorial Atlantic during the last 150,000 years: Results from individual foraminifera. *Paleoceanography and Paleoclimatology*, *11*(2), 217–238.

Bird, C., Darling, K. F., Russell, A. D., Fehrenbacher, J., Davis, C. V., Free, A., & Ngweny, B. (2018). 16S rRNA gene metabarcoding and TEM reveals different ecological strategies within the genus Neogloboquadrina (planktonic foraminifer). *PLoS One*, *13*(1). https://doi.org/10.1371/journal.pone.0191653

Bolton, A., & Marr, J. P. (2013). Trace element variability in crust-bearing and non crust-bearing Neogloboquadrina incompta, P-D intergrade and Globoconella inflata from the Southwest Pacific Ocean: Potential paleoceanographic implications. *Marine Micropaleontology*, *100*, 21–33.

Bonnin, E. A., Zhu, Z. H., Fehrenbacher, J. S., Russell, A. D., Honisch, B., Spero, H. J., & Gagnon, A. C. (2019). Submicron sodium banding in cultured planktic foraminifera shells. *Geochimica et Cosmochimica Acta*, *253*, 127–141.

Boyle, E. A., & Keigwin, L. D. (1985/1986). Comparison of Atlantic and Pacific paleochemical records for the last 250,000 years: Changes in deep ocean circulation and chemical inventory. *Earth and Planetary Science Letters*, *76*, 135–150.

Branson, O., Fehrebnacher, J. S., Vetter, L., Sadekov, A. Y., Eggins, S. M., & Spero, H. J. (2019). LAtools: A data analysis package for the reproducible reduction of LA-ICPMS data. *Chemical Geology*, *504*, 83–95. https://doi.org/10.1016/j.chemgeo.2018.10.029

Brummer, G. J. A., Hemleben, C., & Spindler, M. (1986). Planktonic foraminiferal ontogeny and new perspectives for micropalaeontology. *Nature*, *319*(6048), 50–52.

Brummer, G. J. A., Hemleben, C., & Spindler, M. (1987). Ontogeny of extant spinose planktonic-foraminifera (Globigerinidae)—A concept exemplified by Globigerinoides-sacculifer (Brady) and G-ruber (Dorbigny). *Marine Micropaleontology*, *12*(4), 357–381.

Cleroux, C., deMenocal, P., Arbuszewski, J., & Linsley, B. (2013). Reconstructing the upper water column thermal structure in the Atlantic Ocean. *Paleoceanography and Paleoclimatology*, *28*(3), 503–516. https://doi.org/10.1002/palo.20050

de Nooijer, L. J., Hathorne, E. C., Reichart, G. J., Langer, G., & Bijma, J. (2014). Variability in calcitic Mg/Ca and Sr/Ca ratios in clones of the benthic foraminifer Ammonia tepida. *Marine Micropaleontology*, *107*, 32–43.

Dekens, P. S., Lea, D. W., Pak, D. K., & Spero, H. J. (2002). Core top calibration of Mg/Ca in tropical foraminifera: Refining paleotemperature estimation. *Geochemistry, Geophysics, Geosystems*, *3*(4). https://doi.org/10.1029/2001GC000200

Eggins, S., Sadekov, A., & Deckker, P. D. (2004). Modulation and daily banding of Mg/Ca in *Orbulina universa* tests by symbiont photosynthesis and respiration: A complication for seawater thermometry? *Earth and Planetary Science Letters*, *225*, 411–419.

Emiliani, C. (1955). Pleistocene temperatures. *The Journal of Geology*, *63*(6), 538–578.

Evans, D., Wade, B. S., Henehan, M., Erez, J., & Muller, W. (2016). Revisiting carbonate chemistry controls on planktic foraminifera Mg/Ca: Implications for sea surface temperature and hydrology shifts over the Paleocene Eocene Thermal Maximum and Eocene Oligocene transition. *Climate of the Past*, *12*(4), 819–835.

Fehrenbacher, J. F., & Martin, P. (2014). Exploring the dissolution effect on the intrashell Mg/Ca variability of the planktic foraminifer *Globigerinoides ruber*. *Paleoceanography and Paleoclimatology*, *29*, 854–868. https://doi.org/10.1002/2013PA002571

Fehrenbacher, J. S., Spero, H. J., Russell, A. D., Vetter, L., & Eggins, S. (2015). Optimizing LA-ICP-MS analytical procedures for elemental depth profiling of foraminifera shells. *Chemical Geology*, *407*, 2–9.

Fehrenbacher, J. S., Russell, A. D., Davis, C. V., Spero, H. J., Chu, E., & Hönisch, B. (2018). Ba/Ca ratios in the non-spinose planktic foraminifer Neogloboquadrina dutertrei: Evidence for an organic aggregate microhabitat. *Geochimica et Cosmochimica Acta*, *236*, 361–372. https://doi.org/10.1016/j.gca.2018.03.008

Ford, H. L., Ravelo, A. C., & Polissar, P. J. (2015). Reduced El Nino-Southern Oscillation during the Last Glacial Maximum. *Science*, *347*(6219), 255–258.

Fritz-Endres, T., Dekens, P. S., Fehrenbacher, J., Spero, H. J., & Stine, A. (2019). Application of individual foraminifera Mg/Ca and delta O-18 analyses for paleoceanographic reconstructions in active depositional environments. *Paleoceanography and Paleoclimatology*, *34*(10), 1610–1624.

Gastrich, M. D. (1987). Ultrastructure of a new intracellular symbiotic alga found within planktonic foraminifera. *Journal of Phycology*, *23*(4), 623–632.

Groeneveld, J., Ho, S. L., Mackensen, A., Mohtadi, M., & Laepple, T. (2019). Deciphering the variability in Mg/Ca and stable oxygen isotopes of individual foraminifera. *Paleoceanography and Paleoclimatology*, *34*(5), 755–773. https://doi.org/10.1029/2018PA003533

Hales, B. (2003). Respiration, dissolution, and the lysocline. *Paleoceanography and Paleoclimatology*, *18*(4). https://doi.org/10.1029/2003PA000915

Hathorne, E. C., James, R. H., & Lampitt, R. S. (2009). Environmental versus biomineralization controls on the intratest variation in the trace element composition of the planktonic foraminifera G. inflata and G. scitula. *Paleoceanography and Paleoclimatology*, *24*. https://doi.org/10.1029/2009PA001742

Henehan, M. J., Rae, J. W. B., Foster, G. L., Erez, J., Prentice, K. C., Kucera, M., et al. (2013). Calibration of the boron isotope proxy in the planktonic foraminifera Globigerinoides ruber for use in palaeo-CO_2 reconstruction. *Earth and Planetary Science Letters*, *364*, 111–122. https://doi.org/10.1016/j.epsl.2012.12.029

Hollstein, M., Mohtadi, M., Rosenthal, Y., Sanchez, P. M., Oppo, D., Mendez, G. M., et al. (2017). Stable oxygen isotopes and Mg/Ca in planktic foraminifera from modern surface sediments of the Western Pacific Warm Pool: Implications for thermocline reconstructionsm. *Paleoceanography and Paleoclimatology*, *32*(11), 1174–1194. https://doi.org/10.1002/2017PA003122

Jochum, K. P., Weis, U., Stoll, B., Kuzmin, D., Yang, Q., Raczek, I., et al. (2011). Determination of reference values for NIST SRM 610-617 glasses following ISO guidelines. *Geostandards and Geoanalytical Research*, *35*(4), 397–429.

Johnstone, H. J. H., Schulz, M., Barker, S., & Elderfield, H. (2010). Inside story an X-ray computed tomography method for assessing dissolution in the tests of planktonic foraminifera. *Marine Micropaleontology*, *77*(1–2), 58–70.

Jonkers, L., Buse, B., Brummer, G. J., & Hall, I. R. (2016). Chamber formation leads to Mg/Ca banding in the planktonic foraminifer *Neogloquadrina pachyderma*. *Earth and Planetary Science Letters*, *451*, 177–184.

Jonkers, L., de Nooijer, L. J., Reichart, G. J., Zahn, R., & Brummer, G. J. A. (2012). Encrustation and trace element composition of *Neogloboquadrina dutertrei* assessed from single chamber analyses - implications for paleotemperature estimates. *Biogeosciences*, *9*(11), 4851–4860.

Koutavas, A., & Joanides, S. (2012). El Nino-Southern Oscillation extrema in the Holocene and Last Glacial Maximum. *Paleoceanography and Paleoclimatology*, *27*. https://doi.org/10.1029/2012PA002378

Krupinski, N. B. Q., Russell, A. D., Pak, D. K., & Paytan, A. (2017). Core-top calibration of B/Ca in Pacific Ocean Neogloboquadrina incompta and Globigerina bulloides as a surface water carbonate system proxy. *Earth and Planetary Science Letters*, *466*, 139–151.

Kunioka, D., Shirai, K., Takahata, N., Sano, Y., Toyofuku, T., & Ujiie, Y. (2006). Microdistribution of Mg/Ca, Sr/Ca, and Ba/Ca ratios in *Pulleniatina obliquiloculata* test by using a NanoSIMS: Implication for the vital effect mechanism. *Geochemistry, Geophysics, Geosystems*, *7*, 11. https://doi.org/10.1029/2006GC001280

Lea, D. W., Pak, D. K., & Spero, H. J. (2000). Climate impact of late quaternary equatorial Pacific sea surface temperature variations. *Science*, *289*(5485), 1719–1724.

Longerich, H. P., Jackson, S. E., & Gunther, D. (1996). Laser ablation inductively coupled plasma mass spectrometric transient signal data acquisition and analyte concentration calculation. *Journal of Analytical Atomic Spectrometry*, *11*(9), 899–904.

Marchitto, T. M. (2006). Precise multielemental ratios in small foraminiferal samples determined by sector field ICP-MS. *Geochemistry, Geophysics, Geosystems*, *7*. https://doi.org/10.1029/2005GC001018

Marr, J. P., Bostock, H. C., Carter, L., Bolton, A., & Smith, E. (2013). Differential effects of cleaning procedures on the trace element chemistry of planktonic foraminifera. *Chemical Geology*, *351*, 310–323. https://doi.org/10.1016/j.chemgeo.2013.05.019

McCorkle, D. C., Martin, P. A., Lea, D. W., & Klinkhammer, G. P. (1995). Evidence of a dissolution effect on benthic foraminiferal shell chemistry - delta-C-13, CD/CA, BA/CA, and SR/CA results from the Ontong Java Plateau. *Paleoceanography and Paleoclimatology*, *10*(4), 699–714.

Oba, T. (1990). *Paleoceanographic information obtained by the isotopic measurement of individual foraminiferal specimens.* Proceedings of First International Conference on Asian Marine Geology., Beijing, China: China Ocean Press.

Regenberg, M., Regenberg, A., Garbe-Schonberg, D., & Lea, D. W. (2014). Global dissolution effects on planktonic foraminiferal Mg/Ca ratios controlled by the calcite-saturation state of bottom waters. *Paleoceanography and Paleoclimatology*, *29*(3), 127–142. https://doi.org/10.1002/2013PA002492

Reynolds, C. E., Richey, J. N., Fehrenbacher, J. S., Rosenheim, B. E., & Spero, H. J. (2018). Environmental controls on the geochemistry of Globorotalia truncatulinoides in the Gulf of Mexico: Implications for paleoceanographic reconstructions. *Marine Micropaleontology*, *142*, 92–104.

Rongstad, B. L., Marchitto, T. M., & Herguera, J. C. (2017). Understanding the effects of dissolution on the Mg/Ca paleothermometer in planktic foraminifera: Evidence from a novel individual foraminifera method. *Paleoceanography and Paleoclimatology*, *32*(12), 1386–1402. https://doi.org/10.1002/2017PA003179

Rongstad, B. L., Marchitto, T. M., Marks, G. S., Koutavas, A., Mekik, F., & Ravelo, A. C. (2020). Investigating ENSO-related temperature variability in equatorial pacific core-tops using Mg/Ca in individual planktic foraminifera. *Paleoceanography and Paleoclimatology*, *35*(2). https://doi.org/10.1029/2019PA003774

Russell, A. D., Honisch, B., Spero, H. J., & Lea, D. W. (2004). Effects of seawater carbonate ion concentration and temperature on shell U, Mg, and Sr in cultured planktonic foraminifera. *Geochimica et Cosmochimica Acta*, *68*(21), 4347–4361.

Rustic, G. T., Koutavas, A., Marchitto, T. M., & Linsley, B. K. (2015). Dynamical excitation of the tropical Pacific Ocean and ENSO variability by Little Ice Age cooling. *Science*, *350*(6267), 1537–1541.

Sadekov, A., Eggins, S. M., & De Deckker, P. (2005). Characterization of Mg/Ca distributions in planktonic foraminifera species by electron microprobe mapping. *Geochemistry, Geophysics, Geosystems*, *6*(12). https://doi.org/10.1029/2005GC000973

Sadekov, A., Eggins, S. M., De Deckker, P., & Kroon, D. (2008). Uncertainties in seawater thermometry deriving from intratest and intertest Mg/Ca variability in Globigerinoides ruber. *Paleoceanography and Paleoclimatology*, *23*(1). https://doi.org/10.1029/2007PA001452

Sadekov, A., Eggins, S. M., De Deckker, P., Ninnemann, U., Kuhnt, W., & Bassinot, F. (2009). Surface and subsurface seawater temperature reconstruction using Mg/Ca microanalysis of planktonic foraminifera *Globigerinoides ruber, Globigerinoides sacculifer*, and *Pulleniatina obliquiloculata*. *Paleoceanography and Paleoclimatology*, *24*(3). https://doi.org/10.1029/2008PA001664

Sadekov, A. Y., Eggins, S. M., Klinkhammer, G. P., & Rosenthal, Y. (2010). Effects of seafloor and laboratory dissolution on the Mg/Ca composition of Globigerinoides sacculifer and Orbulina universa tests—A laser ablation ICPMS microanalysis perspective. *Earth and Planetary Science Letters*, *292*(3-4), 312–324. https://doi.org/10.1016/j.epsl.2010.01.039

Schiffelbein, P., & Hills, S. (1984). Direct assessment of stable isotope variability in planktonic-foraminifera populations. *Palaeogeography, Palaeoclimatology, Palaeoecology*, *48*(2–4), 197–213.

Schmitt, A., Elliot, M., Thirumalai, K., La, C., Bassinot, F., Petersen, J., et al. (2019). Single foraminifera Mg/Ca analyses of past glacial-interglacial temperatures derived from G. ruber sensu stricto and sensu lato morphotypes. *Chemical Geology*, *511*, 510–520.

Shuxi, C., & Shackleton, N. J. (1990). New technique for study on isotopic fractionation between sea water and foraminiferal growing processes. *Chinese Journal of Oceanology and Limnology*, *8*(4), 299–305.

Sosdian, S. M., Greenop, R., Hain, M. P., Foster, G. L., Pearson, P. N., & Lear, C. H. (2018). Constraining the evolution of Neogene ocean carbonate chemistry using the boron isotope pH proxy. *Earth and Planetary Science Letters*, *498*, 362–376.

Spero, H. J. (1988). Ultrastructural examination of chamber morphogenesis and biomineralization in the planktonic foraminifer *Orbulina universa*. *Marine Biology*, *99*, 9–20.

Spero, H. J., Eggins, S., Russell, A. D., Vetter, L., Kilburn, M. R., & Honisch, B. (2015). Timing and mechanism for intratest Mg/Ca variability in a living planktic foraminifer. *Earth and Planetary Science Letters*, *409*, 32–42.

Spero, H. J., & Lea, D. W. (1993). Intraspecific stable-isotope variability in the planktic foraminifera globigerinoides-sacculifer—Results from laboratory experiments. *Marine Micropaleontology*, *22*(3), 221–234.

Spero, H. J., & Williams, D. F. (1990). Evidence for seasonal low-salinity surface waters in the gulf of Mexico over the last 16,000 years. *Paleoceanography and Paleoclimatology*, *5*(6), 963–975. https://doi.org/10.1029/PA005i006p00963

Steinhardt, J., de Nooijer, L. L. J., Brummer, G. J., & Reichart, G. J. (2015). Profiling planktonic foraminiferal crust formation. *Geochemistry, Geophysics, Geosystems*, *16*(7), 2409–2430.

Stott, L. D. (1992). Higher temperatures and lower oceanic pCO(2): A climate enigma at the end of the paleocene epoch. *Paleoceanography and Paleoclimatology*, *7*(4), 395–404. https://doi.org/10.1029/92PA01183

Thirumalai, K., Partin, J. W., Jackson, C. S., & Quinn, T. M. (2013). Statistical constraints on El Nino Southern Oscillation reconstructions using individual foraminifera: A sensitivity analysis. *Paleoceanography and Paleoclimatology*, *28*(3), 401–412. https://doi.org/10.1002/palo.20037

Vetter, L., Spero, H. J., Russell, A. D., & Fehrenbacher, J. S. (2013). LA-ICP-MS depth profiling perspective on cleaning protocols for elemental analyses in planktic foraminifers. *Geochemistry, Geophysics, Geosystems*, *14*(8), 2916–2931. https://doi.org/10.1002/ggge.20163

Vetter, L., Spero, H. J., Eggins, S. M., Williams, C., & Flower, B. P. (2017). Oxygen isotope geochemistry of Laurentide ice-sheet meltwater across Termination I. *Quaternary Science Reviews*, *178*, 102–117.

White, S. M., Ravelo, A. C., & Polissar, P. J. (2018). Dampened El Nino in the early and mid-Holocene due to insolation-forced warming/deepening of the thermocline. *Geophysical Research Letters*, *45*(1), 316–326.

Wit, J. C., Reichart, G. J., Jung, S. J. A., & Kroon, D. (2010). Approaches to unravel seasonality in sea surface temperatures using paired single-specimen foraminiferal delta(18)O and Mg/Ca analyses. *Paleoceanography and Paleoclimatology*, *25*. https://doi.org/10.1029/2009PA001857